SUB-RESOLUTION PERMANENT SHADOWING ON AIRLESS BODIES. P. O'Brien[1] and S. Byrne[1], [1]Lunar and Planetary Laboratory, University of Arizona, Tucson, AZ 85721 (pob@lpl.arizona.edu).

Introduction: Ice has long been predicted to exist in cold, Permanently Shadowed Regions (PSRs) on low-obliquity bodies like the Moon, Mercury, and Ceres [1]. These ancient volatile reservoirs are an important constraint on the delivery of water to the inner solar system and its role in establishing planetary habitability as well as a crucial, accessible resource for future human exploration. Near the rotational poles on these bodies, topographic features like crater rims cast shadows that persist indefinitely. In the absence of direct sunlight, PSRs reach temperatures as low as 30 K [2]. Water and other volatile molecules delivered by comets and asteroids will hop ballistically across the surface until they are lost to space or land in a shadowed cold trap where they remain thermally stable against sublimation for billions of years. Ground-based and remote sensing observations over the past few decades have confirmed the presence of volatile-rich polar deposits on each of these bodies through various methods; e.g. radar [3], surface reflectance [4], visible imaging [5], and infrared/neutron spectroscopy [6-8].

Recent work has shown that cold traps can exist in shadows as small as a few tens of centimeters across [9,10], i.e. too small to be observed in current datasets. Ice in PSRs is an invaluable record of solar system history; yet, we do not fully understand the abundance or distribution of sub-resolution shadows that preserve this ice. Here we present preliminary results from a landscape evolution model used to test the hypothesis that small-scale permanently shadowed regions are an important volatile reservoir on airless bodies.

Sub-resolution PSRs: Previous studies have combined illumination models with topography from laser altimetry and imagery to map the largest PSRs on the Moon [11], Mercury [12,13], and Ceres [14], but were ultimately limited by the resolution of available topographic data. [11] catalogued the area of all shadows larger than 1 km^2 on the Moon and the lunar PSR size-frequency distribution is well-fit by a power law that can be extrapolated to smaller shadow sizes (Figure 1). This approach predicts that shadows between 1 m^2 and 1 km^2 in area constitute ~73% of the total shadowed area in the northern hemisphere and ~46% of the total in the southern hemisphere. Sub-km^2 PSRs are likely abundant on all airless bodies and may contribute substantially to the total area where ice could be sequestered.

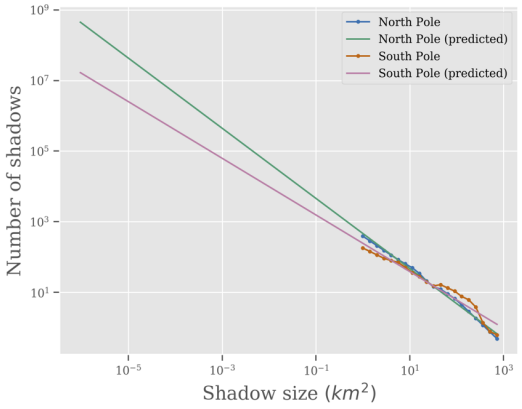

Figure 1. Lunar PSR size-frequency distribution, extrapolated with a power law fit to measurements from [11].

Methods: To constrain the abundance of sub-km^2 permanently shadowed regions, we use a landscape evolution model capable of generating synthetic topography at any scale. For airless bodies, the number of processes acting to modify the surface is small; dominantly, topographic relief-creation from impact cratering and relief-reduction from micrometeorite gardening and seismic shaking, which can collectively be modeled as landscape diffusion [15]. Our model simulates landscapes evolving over time under these processes (Figure 2), incorporating the best approaches of previous studies [16,17] with advancements in physical realism that make it uniquely suited to the study of small permanently shadowed regions.

Impacts are randomly sampled from the impact and velocity distributions of [18], converted to final crater dimensions via the pi-group scaling method [19], and added to random positions on the grid as parabolic bowls with raised rims [17]. We explicitly include the effect of secondary craters produced by large impacts near the model grid following empirical observations of secondary production [20,21]. At each timestep, downslope movement of material is applied by solving the 2D diffusion equation using an alternating direction semi-implicit method [22].

One advantage of this model is that the surface roughness of the final landscape is controlled by the relative rate of cratering and diffusive erosion. Higher diffusivity causes topographic features to erode faster, producing smoother landscapes. The diffusivity can therefore be tuned such that the roughness of our model surfaces matches the roughness of the real surface of the

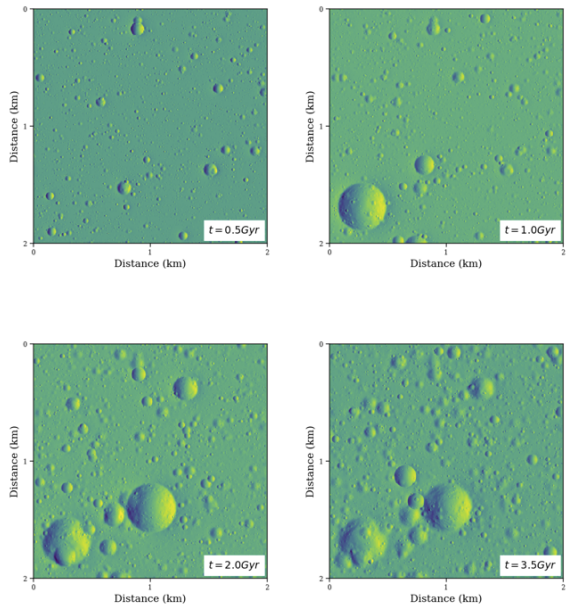

Figure 2. Shaded relief from an example lunar model surface evolving over 3.5 Gyr.

Moon, Mercury, or Ceres. For the present study, roughness is characterized by the median slope and the Hurst parameter, which describes how slopes vary with changes in horizontal baseline. By running the model over a range of diffusivities and comparing the median slopes of the surfaces to those measured using available topography data, we can identify the diffusivity that best matches the polar regions of each body (Figure 3).

Permanently shadowed regions on our model surfaces are determined using the horizon method for illumination [11]. We take a conservative approach and identify only areas where no part of the solar disc is ever visible at a given obliquity.

Results: Using the calibrated model diffusivity for each body (or multiple diffusivities for each body if substantial regional differences in roughness are found), we generate many high-resolution model landscapes corresponding to the polar regions of the Moon, Mercury, and Ceres. By identifying the size and number of all permanently shadowed regions on our model surfaces, we can produce an average size-frequency distribution of PSRs for each body. Our results for the abundance of sub-km^2 shadows will be compared to predictions from previous studies [11-14].

While the present-day axial tilts of these bodies are low enough to permit the presence of shadowed cold traps, these areas are only permanently shadowed so long as axial tilt remains fixed. Ceres has been shown to undergo substantial obliquity cycles with a period of a few tens of kyr [23]. We will explore how the extent of persistent shadowing at sub-km^2 scales varies with changes in obliquity.

In addition to the size and number of sub-spacecraft resolution PSRs, we explore the statistical distribution of other shadow properties such as average depth and sky viewing angle. These parameters have implications for the scattered illumination and maximum temperature within each shadow which in turn control whether a given PSR will be cold enough to trap water ice or other volatile species [24-26].

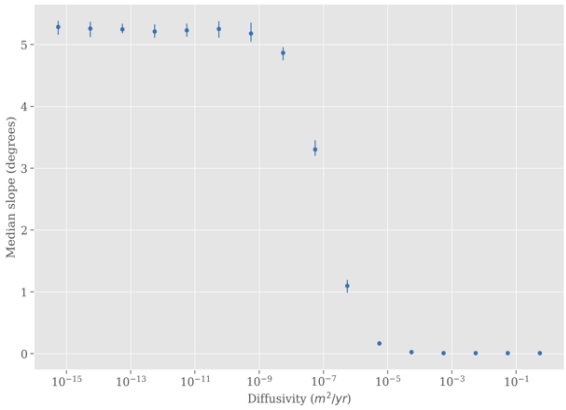

Figure 3. Model surface roughness vs. diffusivity on the Moon, with lines showing interquartile range over many runs at each diffusivity.

References: [1] Watson, K. et al. (1961) *JGR*, 66, 1598-1600. [2] Paige, D.A. et al. (2010) *Science*, 330, 479-482. [3] Butler, B.J. et al. (1993) *JGR*, 98, 15003-15023. [4] Neumann, G.A. et al. (2013) Science, 339, 296-300. [5] Platz, T. et al. (2016) *Nat. Astron.*, 1, 0007. [6] Feldman, W.C. et al. (1998) *Science*, 281, 1496-1500. [7] Colaprete, A. et al. (2010) *Science*, 330, 463-468. [8] Li, S. et al. (2018) *Proc. Natl. Acad. Sci.*, 115, 8907-8912. [9] Hayne, P.O. et al. (2013) *DPS*, 45. [10] Rubanenko, L. et al. (2018) *JGR: Planets*, 8, 2178-2191. [11] Mazarico, E. et al. (2011), *Icarus*, 211, 1066-1081. [12] Chabot, N.L. et al. (2012) *GRL*, 39, L09204. [13] Deutsch, A.N. et al. (2016) *Icarus*, 280, 158-171. [14] Schorghofer, N. et al. (2016) *GRL*, 43, 6783-6789. [15] Soderblom, L.A. (1970) *JGR*, 75, 2655-2661. [16] Howard, A.D. (2007) *Geomorph.*, 91, 332-363. [17] Richardson, J.E. (2009) *Icarus*, 204, 697-715. [18] Marchi, S. et al. (2009) *Astr. Journal*, 137, 4936-4948. [19] Holsapple, K.A. and Housen, K.R. (2007) *Icarus*, 191, 586-597. [20] Vickery, A.M. (1987) *GRL*, 14, 726-729. [21] McEwen, A.S. and Bierhaus, E.B. (2006) *Ann. Rev. Earth and Plan. Sci.*, 34, 535-567. [22] Pelletier, J.D. (2008) *Cambridge*. [23] Ermakov, A.I. et al. (2017) *GRL*, 44, 2652-2661. [24] Vasavada, A.R. et al. (1999) *Icarus*, 141, 179-193. [25] Hayne, P.O. and Aharonson, O. (2015) *JGR: Planets*, 120, 1567-1584. [26] Rubanenko, L. and Aharonson, O. (2017) *Icarus*, 296, 99-109.